Inorganic Chemistry

Article

pubs.acs.org/IC

Radical-Based Epoxide Opening by Titanocenes

Asli Cangönül,[†] Maike Behlendorf,[‡] Andreas Gansäuer,*[,‡] and Maurice van Gastel*[,†]

[†]Max Planck Institute for Chemical Energy Conversion, Stiftstrasse 34-36, D-45470 Mülheim an der Ruhr, Germany

[‡]Kekulé-Institut für Organische Chemie und Biochemie der Universität Bonn, Gerhard Domagk Str. 1, 53121 Bonn, Germany

Supporting Information

ABSTRACT: The binding of 2,2-diphenyloxirane to Cp_2TiCl is studied on the electronic level by magnetic resonance spectroscopy and quantum chemical calculations. The complexation of 2,2-diphenyloxirane is accompanied by dissociation of the chloride ligand, and thus, the epoxide binds to the cationic titanocene(III) complex. The titanocene(III)−epoxide species persists only for short periods of time (<5 min) even at 243 K, indicating that the ring-opening reaction is exothermic. A short-lived paramagnetic titanocene(IV)−epoxide radical species has not been directly observed. However, by a combination of isotope labeling and spin-trapping, evidence for the existence of such a species has been unequivocally demonstrated. The observation of a titanocene(III)−epoxide complex is unprecedented and provides direct evidence for inner-sphere electron transfer between epoxides and titanocenes, responsible for the high regioselectivity of ring-opening.

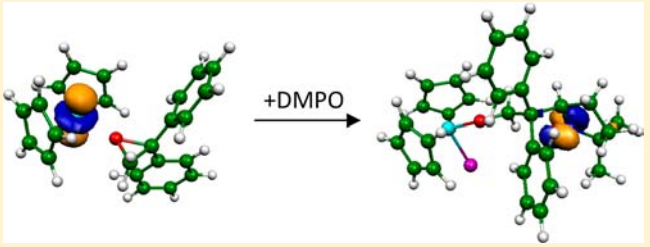

INTRODUCTION

Free radicals are reactive intermediates of considerable importance in organic chemistry.[1−5] The main advantages of radical chemistry are the mildness of radical generation, the wide applicability to many functional groups, and the high predictability of C−C bond-forming reactions.[3] Also, they are usually stable under protic conditions. As a result, the number of protocols for the application of radicals in synthesis is growing steadily.[6,7]

A disadvantage of chain reactions concerns the lack of reagent-controlled stereoselectivity of the radical reaction.[8] This is because the initiator does not bind to the radical precursor or the radical itself. Reagent control in radical reactions can be exerted if a metal complex can activate a suitable radical precursor for radical formation and then remain bound to the radical formed. This approach is especially attractive if the metal complex can be employed catalytically. To this end, epoxides have been used as radical precursors with titanocene(III) complexes as electron-transfer catalysts for reagent-controlled radical reactions with some success.[9−11] Examples of the catalytic reactions[12−15] are enantioselective and regiodivergent epoxide openings,[16−22] epoxypolyene cyclizations via radicals,[23−27] unusual radical cyclizations,[28−32] and, more recently, catalytic atom-economical reactions.[33−37] The catalytic reactions are based on the seminal stoichiometric transformations introduced by Nugent and RajanBabu.[38−41] The use of titanocene bound ketyl radicals in reagent-controlled catalytic reactions is an emerging area of research,[42−47] and the first enantioselective cyclization has been reported only recently.[48,49] Also, styrene polymerizations via radicals have been initiated by titanocene-mediated epoxide opening.[50,51]

Despite the many highly selective reactions based on titanocene-mediated reductive epoxide opening, the reaction mechanism has so far only been studied computationally and by analysis of the products' distribution,[52,53] and hence, the identity of the reaction intermediates and their electronic properties remain to be experimentally verified. In this contribution, we address this issue by employing electron paramagnetic resonance (EPR) spectroscopy.

EPR spectroscopy is a perfect method for this purpose, since it allows for the selective and sensitive detection of paramagnetic reaction intermediates without additional signals of diamagnetic compounds. The spectroscopic signature in EPR spectroscopy, the set of three g values, provides critical information of the singly occupied molecular orbital and whether it is metal-centered or centered on an organic molecule. Additionally, we use the hyperfine resolving techniques electron spin echo envelope modulation (ESEEM)[54−56] and pulsed electron nuclear double resonance (ENDOR),[57−59] which, in combination with isotope labeling, are well-suited to obtain information about the electronic and geometric structure of the radical intermediates. Whereas the ENDOR technique is ideally suited for the detection of nuclei with large gyromagnetic ratios for which the transition frequencies are much higher than 0 MHz, ESEEM spectroscopy is sensitive to nuclei whose transition frequencies are typically below 5 MHz. The magnitude of the hyperfine interaction reveals information about the effective distance between the unpaired electron at titanium and the nuclear spin and, more importantly, in the case of isotope labeling, can immediately be used to verify the binding mode of the paramagnetic species. In

Received: June 3, 2013
Published: October 10, 2013

   dx.doi.org/10.1021/ic401403a | *Inorg. Chem.* 2013, 52, 11859−11866

our case, this provides the unique opportunity to identify the elusive epoxide titanocene(III) complex.

Although EPR spectroscopy can, in principle, be used to detect short-lived radical intermediates, its present absolute sensitivity typically amounts to 10^8 paramagnetic species. The lifetime of carbon-centered radicals is typically very short, and thus, the buildup of radicals in a large enough quantity for a direct detection may not be possible. A way to circumvent this problem is to transform highly reactive radicals into more stable species with increased lifetime by means of spin-trapping.

With the spin-trapping technique,[60−63] the short-lived radical reacts with a diamagnetic compound, which generally contains a nitroso group that takes over the radical and forms a more stable nitroxide radical adduct. In this work, 5,5-dimethyl-1-pyrroline-*N*-oxide (DMPO) has been used (see Scheme 1).[64]

Scheme 1. DMPO and Spin-Trapping

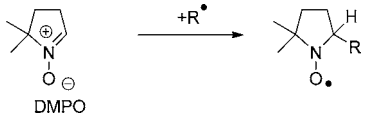

For DMPO, the C═N double bond is subject to nucleophilic attack by short-lived radicals R•, thus giving rise to the nitroxide radical adduct with the original radical R covalently bound to the neighboring carbon atom (Scheme 1).

MATERIAL AND METHODS

Sample Preparation. All samples were prepared under an argon atmosphere using standard Schlenk techniques. The solvent THF was distilled prior to use from sodium and benzophenone. Although this procedure is routinely used for solvent purification, it is only partially effective to remove H_2O.[65] Cp_2TiCl_2 (Aldrich), (2,2,6,6-tetramethylpiperidin-1-yl)oxidanyl (TEMPO) (Aldrich), DMPO (Aldrich), 2,2-diphenyloxirane (Acros), and dicyclopentadiene (Aldrich) were purchased and used as received. 2,2-Diphenyloxirane was used as a prototypical epoxide owing to its small size and since deuterium isotope labeling of the two methylene protons can be selectively performed. Additionally, when opened, the structure is as close as possible to a trityl moiety, which prolongs the lifetime of short-lived radical species such that they can be optimally spin-trapped.

Cyclopentadiene-D_6 was prepared by following the method of Lambert and Finzel:[66] Na (8.40 g, 365 mmol) was added to 80 mL of D_2O, and the mixture was cooled to 0 °C at a slow enough rate to keep the temperature below 10 °C. After addition was complete, 40 mL was syringed into a flask containing freshly cracked C_5H_6 (28.30 g, 428 mmol) in DMSO (40 mL) at 0 °C. The mixture was stirred vigorously for 1 h. Subsequently, the resulting layers were separated, and the top C_5H_6 layer was syringed into another flask containing 40 mL of NaOD/D_2O solution in DMSO (40 mL) at 0 °C. The mixture was again stirred for 1 h, and separation and stirring was repeated for a third time.

$(C_5D_5)TiCl_2$ was prepared as follows:[67] $TiCl_4$ (3.80 g, 42 mmol) in THF (90 mL) was cooled to −78 °C. To this solution were dropwise added C_5D_6 (17.45 g, 242 mmol) and $HN(CH_3)_2$ (12.0 g, 266 mmol) in THF (20 mL), and the mixture was heated to 60 °C and then refluxed for 8 h. The solid was separated, washed twice with THF, then with petrol ether, and dried under vacuum. The product was suspended in aqueous HCl (1 M), filtered, washed with water and with methanol, and dried again under vacuum.

D_2-2,2-diphenyloxirane. Following the procedure of Shi et al.:[68] 1,1′-Bis-phenyl (2,2-D_2-ethenylidene) (4.55 g, 25.0 mmol, 97% *D*-incorporation as judged by integration of the ^{1}H NMR signal of the residual CH_2 group) and 375 mg of $NBu_4^+HSO_4^-$ (0.375 g, 1.10 mmol, 4.40 mol %) were dissolved in a 2:1 mixture of CH_3CN and dimethoxymethane (150 mL), 50 mL of acetone (50 mL, 27.2 equiv), and aq K_2CO_3 (1.66 M, 20 mL). By peristaltic pump, solutions of Oxone (46 g in 200 mL of 4×10^{-4} M EDTA solution; 302 mmol, 12.1 equiv) and aq K_2CO_3 (1.66 M, 200 mL) were added simultaneously over a period of 4 h and then stirred overnight. The reaction mixture was extracted with petrol ether and dried over $MgSO_4$. Upon removal of the solvent under reduced pressure, pure D_2-2,2-diphenyloxirane was obtained as colorless solid (4.49 g, 22.6 mmol, 90% yield) that was identical to the 2,2-diphenyloxirane except for the missing signal of the CH_2 group in the ^{1}H and ^{13}C NMR spectra. The degree of deuteration (95%) was judged by integration of the ^{1}H NMR signal of the residual CH_2 group.

A stock solution of Cp_2TiCl was prepared by dissolving Cp_2TiCl_2 in THF to an end concentration of 10 mM and addition of 1 molar equiv of zinc powder.[41] During this reduction, $ZnCl_2$ is formed. ESEEM spectra (vide infra) indicate that the Lewis acidity of $ZnCl_2$ is not sufficient to form the Cp_2Ti^+ species, though it possibly assists in its formation upon the addition of 2,2-diphenyloxirane. Depending on the experiment, 1 or 5 molar equiv of 2,2-diphenyloxirane or D_2-2,2-diphenyloxirane was added to the green solution of Cp_2TiCl in THF at −30 °C. For experiments with spin-trapping, 1 molar equiv of DMPO in THF was added into Cp_2TiCl in THF solution, and after a few seconds, 10 molar equiv of 2,2-diphenyloxirane or deuterated 2,2-diphenyloxirane was added to the solution of Cp_2TiCl and DMPO in THF at room temperature.

In this manner, the following samples have been prepared: (**1**) 10 mM Cp_2TiCl in THF; (**2**) 10 mM Cp_2TiCl in THF and 50 mM 2,2-diphenyloxirane; (**3**) 10 mM Cp_2TiCl in THF and 50 mM D_2-2,2-diphenyloxirane; (**4**) 10 mM $(C_5D_5)TiCl_2$ in D_8-THF with 50 mM 2,2-diphenyloxirane; (**5**) 10 mM Cp_2TiCl in THF and 10 mM DMPO; (**6**) 10 mM Cp_2TiCl in THF with 100 mM 2,2-diphenyloxirane and 10 mM DMPO; (**7**) 10 mM Cp_2TiCl in THF with 100 mM D_2-2,2-diphenyloxirane and 10 mM DMPO; and (**8**) 10 mM TEMPO in THF as a control sample. The solutions were transferred from a Schlenk tube into the EPR tube under Ar and frozen in liquid nitrogen.

Measurements. All EPR, ESEEM, and ENDOR spectra were recorded for frozen solutions (T = 30 K) using a Bruker ELEXSYS E580 and SuperQ FT-EPR spectrometer operating at 9 and 34 GHz, respectively. The EPR and ESEEM experiments were performed with a Bruker MD5 resonator and Davies-ENDOR with an MD4 resonator. For the electron spin echo (ESE) detected EPR experiments at 34 GHz, a Hahn echo pulse sequence with pulses of 24 and 48 ns and a pulse separation of 300 ns was employed. The three-pulse ESEEM[69] experiments at 9 and 34 GHz were carried out with pulses of 16 and 36 ns in length, respectively. An exponential background was subtracted from the modulation pattern. The resulting modulations were multiplied with a Hamming window function, zero-filled to 2048 points and Fourier transformed into frequency domain. The spectra are displayed as magnitude ESEEM spectra. Davies ENDOR spectra have been recorded with a pulse sequence, which features an RF pulse of 10 μs, an inversion pulse of 200 ns, and a Hahn echo detection sequence with pulses of 100 and 200 ns. In the ENDOR experiment, the magnetic field and all microwave pulses are fixed and the frequency of the RF pulse is swept while monitoring the ESE detected EPR signal. The exact RF frequency, at which the echo-signal changes, provides information about the magnitude of the hyperfine interaction. The reason for using two frequency bands is that the different Zeeman frequencies at X- and Q-bands (factor of about 3.5) give rise to a changed ratio of the hyperfine and quadrupole interactions, which, of course, do not change, with respect to the nuclear Zeeman frequencies. As a consequence, signals of, for example, ^{14}N are more pronounced in X-band ESEEM than in Q-band ESEEM spectra, whereas Q-band ESEEM spectra are devoid of contributions of protons, facilitating the assignment of bands. In this respect, the spectra give complementary information, and the band in which a particular effect is more pronounced is chosen for the figures in the article.

For the analysis of the ESEEM data in this article, it is important to realize that the obtained ESEEM spectra display bands, from which it is, in principle, possible to extract information about the hyperfine and quadrupole interactions. However, since the hyperfine tensor is a 6

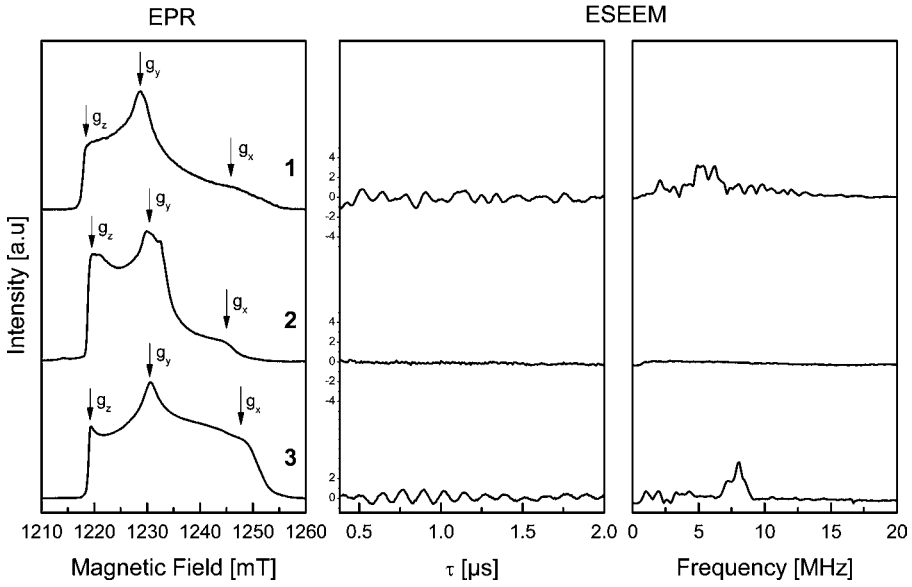

Figure 1. Q-band ESE detected EPR spectra (left), ESEEM modulation patterns recorded at the g_y canonical orientations (middle), and ESEEM spectra (right) of (**1**) Cp_2TiCl in THF, (**2**) Cp_2TiCl in THF and 5 molar equiv of 2,2-diphenyloxirane, and (**3**) Cp_2TiCl in THF and 5 molar equiv of D_2-2,2-diphenyloxirane. Experimental conditions: T = 30 K, ν_{mw} = 34.117 GHz, ESEEM pulse sequence 90°−τ−90°−T−90°−τ−echo, length of 90° pulses 36 ns, τ = 300 ns. The y axis in the middle diagram indicates the modulation amplitude [%]. Signals assigned to deuterium (Zeeman frequency = 8 MHz) are indicated in the ESEEM spectrum of (**3**) with vertical bars.

parameter property and the traceless quadrupole tensor is a 5 parameter property, given the presence of, at most, a few bands in the spectra above the noise level, accurate determination of these 11 parameters is not feasible and would likely even require extended studies of oriented molecules in a host crystal. As an example, an ESEEM simulation of one chloride nucleus alone (I = 3/2) with hyperfine and quadrupole couplings based on DFT calculations is included in the Supporting Information and gives rise to 6 single quantum, 4 double quantum, and 2 triple quantum transitions, that is, 12 bands. We thus prefer not to reduce our data set into sets of nuclear hyperfine and quadrupole parameters by simulations. Determination of nuclear hyperfine and quadrupole parameters is also not the goal of this study. Rather, the directly interpretable, albeit qualitative, information, which also gives the most relevant information about the reaction mechanism, is the observation of whether or not a signal of a particular nucleus (e.g., chloride, vide infra) is present. We thus prefer to refrain to translate our set of data into nuclear hyperfine and quadrupole coupling constants, though a few numbers will be mentioned in the text. If well-defined hyperfine shifted bands are visible in the ESEEM (or ENDOR) spectra, the nucleus must be coordinated to the titanocene, since the remote nuclei would only contribute at the nuclear Zeeman frequency and unspecifically bound ("nearby") nuclei would have a distribution of positions, which would lead to a line broadening to such an extent that the bands become beyond the detection limit. Thus, if well-defined hyperfine shifted bands are present in the spectra, the atom is in a well-defined position with respect to the unpaired electron at the titanium and must thus be coordinated to titanocene; if the ESEEM or ENDOR signal disappears while the g values essentially do not change, the atom is no longer coordinated.

Quantum Chemistry. DFT calculations of models for Cp_2TiCl and 2,2-diphenyloxirane, Cp_2TiCl and DMPO, and Cp_2TiCl with 2,2-diphenyloxirane and DMPO were performed with the ORCA program package.[70] Geometry optimization was carried out with the BP86 functional and a split-valence basis set with additional polarization functions (SVP).[71,72] After geometry optimization, the B3LYP functional and a triple-ζ basis set with polarization functions (Def2-TZVP)[73] were employed to calculate g values and hyperfine coupling constants within a spin-unrestricted Kohn−Sham formalism.[74,75] The Cartesian coordinates of the geometry-optimized structures are given as Supporting Information.

RESULTS AND DISCUSSION

To fully investigate the mechanism of epoxide opening by titanocene, this section is divided in two parts. In the first part, the binding of epoxide to Zn-reduced Cp_2TiCl_2 at 243 K is investigated. In the second part, the epoxide opening process is examined.

Epoxide Binding. Q-band ESE detected EPR spectra (left), three-pulse ESEEM modulation patterns recorded at the g_y canonical orientation (middle), and ESEEM spectra (right) of frozen solutions of (**1**)−(**3**) are shown in Figure 1. The canonical g values read from the EPR spectra are representative for a monomeric, $d^1_{z^2}$ species, which is in agreement with previous observations.[76] The cw EPR spectrum of (**1**) (see the Supporting Information) additionally contains a signal with a g value of 1.945 that has been assigned to the cationic species Cp_2Ti^+.[77] The presence of this signal is a result of trace amounts of H_2O that could not be removed by the distillation procedure.[65] The spectrum of (**2**) is characterized by essentially the same g values as those for Cp_2TiCl, though the intensity of (**3**) has redistributed such that the amplitude at g_x has increased. The observed canonical g values of (**1**)−(**3**) indicate an identical electronic ground state in all compounds. This result is corroborated by DFT calculations (cf. Table 1). Upon prolonged mixing time in (**3**) and (**4**) at room temperature, the EPR signal disappears and the color of the sample becomes red, indicative of a Ti(IV) species.

The ESEEM modulation pattern of (**1**) displays a rich structure. It contains frequencies in the range of 1−15 MHz. Since the proton Zeeman frequency at the Q-band amounts to 50 MHz, the low-frequency signals must stem from a low-γ quadrupolar nucleus. The only nucleus that is compatible with these signals is chloride. For Cp_2TiCl and 2,2-diphenyloxirane (**2**), the echo invariably lacked significant modulations. The complete disappearance of the ESEEM signal upon addition of 2,2-diphenyloxirane indicates that the chloride has dissociated and that the epoxide binds to the cationic Cp_2Ti^+ complex. The

dx.doi.org/10.1021/ic401403a | Inorg. Chem. 2013, 52, 11859−11866

Table 1. Experimental and Calculated Canonical g Values for (1) Cp_2TiCl, (2) Cp_2TiCl and 2,2-diphenyloxirane, (3) Cp_2TiCl and D_2-2,2-diphenyloxirane, and (5) Cp_2TiCl and DMPO

		g_x	g_y	g_z
1	exp	1.952(5)	1.982(2)	2.001(2)
	DFT	1.954	1.985	1.999
2	exp	1.955(5)	1.981(2)	1.999(2)
3	exp	1.948(5)	1.981(2)	2.001(2)
	DFT	1.940	1.989	2.000
5	exp	1.963(5)	1.980(2)	1.998(2)
	DFT	1.965	1.982	2.001

observation of the cationic species as the catalytically relevant complex is in agreement with X-ray studies of the binding of CO_3^- to Cp_2TiCl reported by Rosenthal et al.[78] For Cp_2TiCl with D_2-2,2-diphenyloxirane (**3**), modulations are visible again, but with frequency components at 8 MHz, indicated with vertical bars in Figure 1. The largest amplitude occurs at 8.0 MHz, corresponding to the Zeeman frequency of deuterium. Thus, the presence of modulations at the deuterium Zeeman frequency directly confirms the magnetic coupling of a deuterium nucleus to the unpaired electron at titanium. Additional experiments (see Figure S12, Supporting Information) indicate that unbound "nearby" D_2-2,2-diphenyloxirane would not give rise to detectable deuterium modulations. Thus, the observation of deuterium-derived signals directly confirms the binding of D_2-2,2-diphenyloxirane to titanium.

To obtain more information, X-band modulation patterns and ESEEM spectra of (**2**)−(**4**), recorded at the g_y canonical orientation, have been recorded. They are shown in Figure 2. At the X-band, all signals are located between 0 and 20 MHz. For (**2**), modulations of protons are observed at 15 MHz. For (**3**), these modulations are still present. In addition, a lower frequency at 2 MHz with a large amplitude dominates. In the ESEEM spectrum of (**4**), only the frequency component at 2 MHz remains. The signals at the deuterium Zeeman frequency at 2 MHz in the ESEEM spectra of (**3**) and (**4**) give even further indication of epoxide binding and the displacement of chloride.

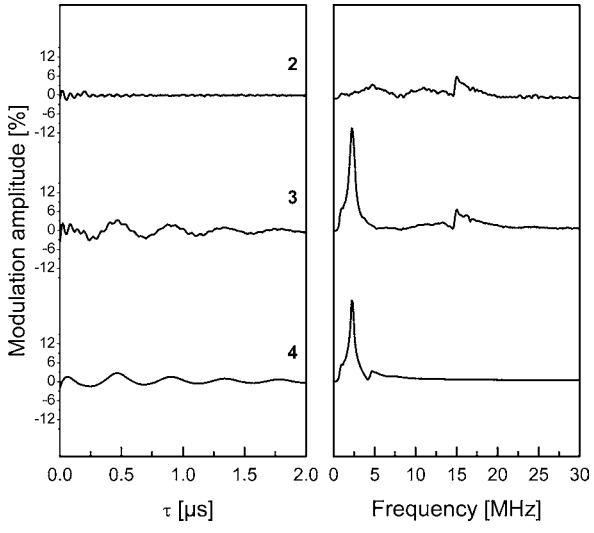

Figure 2. X-band three-pulse modulation patterns recorded at the g_y canonical orientations (left) and ESEEM spectra (right) of (**2**) Cp_2TiCl in THF and 1 molar equiv of 2,2-diphenyloxirane, ν_{mw} = 9.7171 GHz; (**3**) Cp_2TiCl in THF and 1 molar equiv of D_2-2,2-diphenyloxirane, ν_{mw} = 9.7215 GHz; and (**4**) $(C_5D_5)_2TiCl$ in D_8-THF and 1 molar equiv of 2,2-diphenyloxirane, ν_{mw} = 9.726 GHz. Experimental conditions: T = 30 K, pulse sequence 90°−τ−90°−T−90°−τ− echo, length of 90° pulses 16 ns, τ = 200 ns.

In the ESEEM spectra of (**2**) and (**3**), proton signals occur at the proton frequency of 15 MHz (alternatively, these are the fast oscillations in the modulation pattern in the left diagram of Figure 2). They almost completely disappear in the ESEEM spectrum of (**4**), indicating an essentially complete degree of deuteration in the C_5D_5 ligands. This opens the possibility to investigate the proton hyperfine coupling constants of 2,2-diphenyloxirane by complete deuteration of the ligands and THF. X-band Davies ^{1}H ENDOR spectra of (**1**)−(**4**), recorded at the g_y canonical orientation, are shown in Figure 3. The

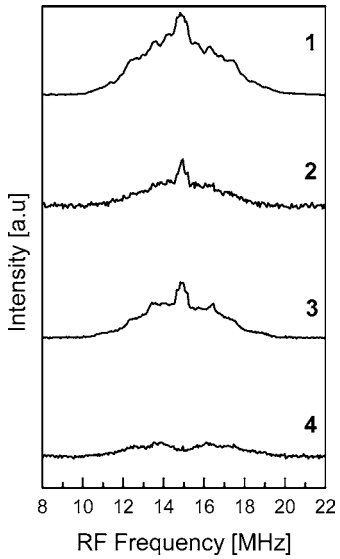

Figure 3. X-band ENDOR spectrum (T = 30 K) of (**1**) Cp_2TiCl in THF, ν_{mw} = 9.7173 GHz; (**2**) Cp_2TiCl in THF and 2,2-diphenyloxirane, ν_{mw} = 9.7171 GHz; (**3**) Cp_2TiCl in THF and D_2-2,2-diphenyloxirane, ν_{mw} = 9.7215 GHz; and (**4**) $(C_5D_5)_2TiCl$ in D_8-THF and 2,2-diphenyloxirane, ν_{mw} = 9.726 GHz, recorded at the g_y canonical orientations. Experimental conditions: RF pulse length 10 μs, length of inversion pulse 200 ns. The total accumulation time for each spectrum amounts to 10 h.

ENDOR signals span the frequency region from 10.2 to 19.9 MHz. The ENDOR spectra of (**1**)−(**3**) are similar in appearance. With C_5D_5 ligands in D_8-THF, the ENDOR spectrum simplifies significantly. The remaining signals in the ENDOR spectrum of (**4**) span a range from 12 to 19 MHz. DFT calculations give rise to principal values of the ^{1}H hyperfine tensor of the epoxide protons of −1.8, −1.7, and +2.3 MHz on a model geometry in which the epoxide binds directly to titanium. Thus, the signals of the epoxide protons are expected in the region from 13.8 to 16.2 MHz. The weak signals below 13.8 MHz and above 16.2 MHz likely stem from trace amounts of H_2O in THF, which has also been observed before by hyperfine sublevel correlation (HYSCORE) spectroscopy.[79]

Spin-Trapping. X-band ESE detected EPR spectra of frozen solutions of (**1**), (**5**), (**6**), and (**8**) are shown in Figure 4. When DMPO is added, the spectrum of (**5**) is characterized by a significantly larger g_x value than that of Cp_2TiCl (see Table 1). The g_x and g_y values are smaller than g_e, indicating that the

dx.doi.org/10.1021/ic401403a | Inorg. Chem. 2013, 52, 11859−11866

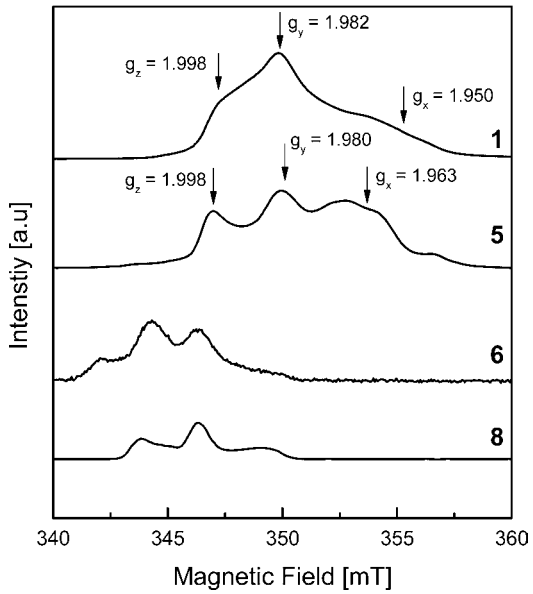

Figure 4. X-Band ESE detected EPR spectra (T = 30 K) of (**1**) Cp_2TiCl in THF, ν_{mw} = 9.7118 GHz; (**5**) $[TiCp_2]^+$ with DMPO in THF; (**6**) $[Cp_2Ti]^+$ with 2,2-diphenyloxirane and DMPO in THF; and (**8**) TEMPO in THF.

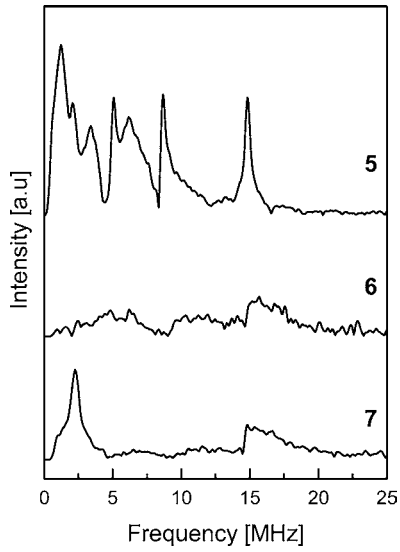

Figure 5. X-band three-pulse ESEEM spectra of (**5**) $[Cp_2Ti]^+$ with DMPO in THF, ν_{mw} = 9.6603 GHz; (**6**) $[Cp_2Ti]^+$ with 2,2-diphenyloxirane and DMPO in THF, ν_{mw} = 9.7221 GHz; and (**7**) $[Cp_2Ti]^+$ with D_2-2,2-diphenyloxirane and DMPO in THF, ν_{mw} = 9.7135 GHz, recorded at the g_y canonical orientations. Experimental conditions: T = 30 K, RF pulse length 10 μs, length of inversion pulse 200 ns.

unpaired electron remains at Ti(III), as confirmed by DFT calculations (see Table 1). A signal of (**1**) remains visible at 357 mT when 1 molar equiv of DMPO is added, indicating that formation of the titatocene−DMPO adduct is not complete, but rather an equilibrium process. Moreover, at the g_x position, a residual hyperfine structure seems to be present in the EPR spectrum of (**5**). A simulation that reproduces the features of the majority species (**5**), but does not accurately reproduce the relative intensities of the absorption line shape, is included in the Supporting Information. Upon addition of 2,2-diphenyloxirane to Cp_2TiCl and DMPO and a mixing time of several minutes, a strong signal with g values typical for nitroxide radicals is observed (see Figure 4, (**6**)). The EPR spectrum compares well to that of the well-known TEMPO radical, also included in Figure 4.[80−82] For a nitroxide radical, the unpaired electron is mainly distributed in a π^* orbital at oxygen and nitrogen. Also, the 2s orbitals of nitrogen and oxygen atoms carry a small amount of spin density. Typical g values and typical ^{14}N hyperfine couplings are g_x = 2.0090, g_y = 2.0060, g_z = 2.024 and A_x = A_y = 18 MHz, A_z = 96 MHz.[80−82] The magnetic parameters can change slightly for different classes of nitroxides, but the z principal axes of the ^{14}N hyperfine and g tensor are nearly coincident.[80−82]

Three-pulse ESEEM spectra of frozen solutions of (**5**)−(**7**) are shown in Figure 5. The signals in the ESEEM spectrum of (**5**) are completely different from those of (**6**) and (**7**) and display a rich structure of six signals below 10 MHz (1.22, 2.08, 3.42, 5.07, 6.16, 8.67 MHz). These six signals of which the first and third frequency approximately add up to the fourth, and the second and fifth frequency add up to give the sixth frequency, are indicative of single quantum and double quantum transitions of a nuclear spin I = 1 nucleus and are, therefore, assigned to the coupling of the unpaired electron to ^{14}N. The bands in the spectrum of complex (**5**) are significantly narrower than those of complexes (**6**) and (**7**). Thus, both the EPR and the ESEEM spectra indicate that DMPO, the only molecule that contains ^{14}N, binds to Ti(III), but the unpaired electron remains located at titanium. Additionally, mass spectroscopy (see the Supporting Information) and DFT calculations support the dissociation of chloride upon binding of DMPO to the cationic Cp_2Ti^+. Strikingly, a large signal at the deuterium Zeeman frequency (2 MHz) is visible in the ESEEM spectrum of (**7**), indicating a magnetic coupling between the unpaired electron at the nitroxide and a deuterium nucleus. This provides the first direct experimental evidence that the radical species that has been trapped by DMPO is formed from 2,2-diphenyloxirane and that the epoxide opens via a radical mechanism.

The singly occupied molecular orbitals (SOMOs) obtained for models of (**2**), (**5**), and (**6**) are shown in Figure 6. The singly occupied $d^1_{z^2}$ orbital at Ti(III) is clearly recognizable for (**2**) and (**5**). Upon inclusion of 2,2-diphenyloxirane to the model geometry of (**1**), it turns out that epoxide bonding cannot be realized due to steric interactions of the phenyl groups with either of the Cp ligands without dissociation of Cl^- from the model structure. For this optimized geometry, a $d^1_{z^2}$ SOMO is found as well. The Ti−O distance amounts to 2.065 Å, and the two C−O distances amount to 1.60 and 1.44 Å and are slightly longer than the optimized distances of 1.45 and 1.43 Å for isolated 2,2-diphenyloxirane.The optimized Ti−O distance amounts to 1.980 Å in (**5**). For complex (**6**), the SOMO comprises the π^* orbital of nitroxide and the Ti−O distance amounts to 1.785 Å. This again confirms the proposed mechanism of reductive epoxide opening. In this structure, both the oxygen atom and the chloride are able to coordinate to Ti(IV). Thus, the DFT calculations fully corroborate experimentally observed dissociation of chloride upon binding of epoxide as well as the reductive epoxide opening by a radical mechanism.

Mechanistic Implications. The mechanistic pictures of the reductive ring-opening reaction of epoxide are shown in Scheme 2. We propose that the reaction is completed in two steps. In the first step, epoxide binds to Cp_2TiCl and chloride

dx.doi.org/10.1021/ic401403a | Inorg. Chem. 2013, 52, 11859−11866

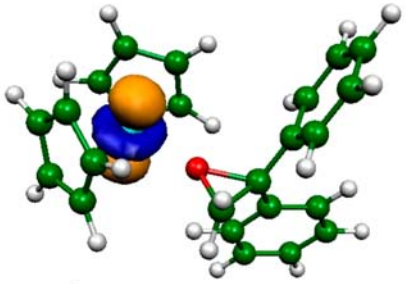

$[Cp_2Ti]^+$ * 2,2-diphenyloxirane(**2**)

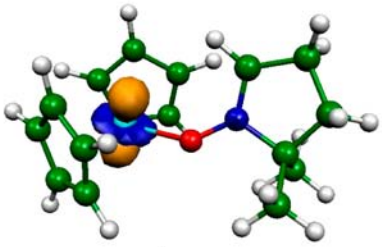

$[Cp_2Ti]^+$ * DMPO (**5**)

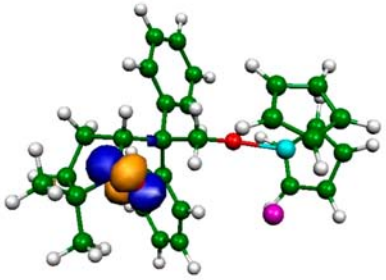

$[Cp_2TiCl]$ * 2,2-diphenyloxirane with DMPO (**6**)

Figure 6. Singly occupied orbitals (SOMOs) for geometry-optimized models (B3LYP functional, SVP basis set)[70,72] of $[Cp_2Ti]^+$ with 2,2-diphenyloxirane (**2**), $[Cp_2Ti]^+$ with DMPO (**5**), and Cp_2TiCl with 2,2-diphenyloxirane and DMPO (**6**). Color code: carbon (green), hydrogen (white), titanium (cyan), chloride (magenta), nitrogen (blue), oxygen (red). The positive and negative contours of the orbital are indicated in orange and blue.

dissociates, thus forming a β-titanoxy (**A**) radical. For the second step, epoxide is reductively opened and a carbon radical (**B** or **C**) is generated. From the DFT calculations, the benzylic radical (**C**) is energetically more favorable by 22.7 kcal mol^{-1} than the primary radical (**B**), in agreement with previous experimental results.[41,53]

In a general perspective, our observations with and without spin-trap experiments reveals important information about the reaction mechanism of the reductive ring-opening of epoxides, a very active field of research. Our work constitutes the first identification of a complex of an epoxide with a low-valent metal complex and provides strong experimental evidence for the postulated inner-sphere electron transfer between epoxides and titanocenes that has been put forward to explain the high regioselectivity of ring-opening. The rather surprising cationic structure—usually pending amide ligands are necessary to provide stabilization for such species[32,83]—of the complex provides an experimental basis for the design of reactions based on enantioselective interactions between epoxides and titanocenes.

■ ASSOCIATED CONTENT

Supporting Information

Additional EPR, ENDOR, and ESEEM spectra of all compounds at the X-band and Cartesian coordinates of optimized models for structures (**1**), (**2**), (**5**), and (**6**). This material is available free of charge via the Internet at http://pubs.acs.org.

■ AUTHOR INFORMATION

Corresponding Authors

*E-mail: andreas.gansaeuer@uni-bonn.de.

*E-mail: maurice.van-gastel@cec.mpg.de.

Notes

The authors declare no competing financial interest.

■ ACKNOWLEDGMENTS

This project is financially supported by the Deutsche Forschungsgemeinschaft (DFG), SFB 813 TP A4 and TP B2, by the University of Bonn and by the Max-Planck Society.

■ REFERENCES

(1) Zard, S. Z. *Radical Reactions in Organic Synthesis*; Oxford University: Oxford, U.K., 2003.

(2) Renaud, P., Sibi, M. P., Eds. *Radicals in Organic Synthesis*; Wiley-VCH: Weinheim, Germany, 2001.

(3) McCarroll, A. J.; Walton, J. C. *Angew. Chem., Int. Ed.* **2001**, *40*, 2225−2250.

(4) Curran, D. P.; Porter, N. A.; Giese, B. *Stereochemistry of Radical Reactions*; VCH: Weinheim, Germany, 1996.

(5) Fossey, J.; Lefort, D.; Sorba, J. *Free Radicals In Organic Synthesis*; Wiley: Chichester, U.K., 1995.

(6) Rowlands, G. J. *Tetrahedron* **2009**, *65*, 8603−8655.

(7) Rowlands, G. J. *Tetrahedron* **2010**, *66*, 1593−1636.

(8) Gansäuer, A.; Bluhm, H. *Chem. Rev.* **2000**, *100*, 2771−2788.

(9) Gansäuer, A.; Lauterbach, T.; Narayan, S. *Angew. Chem., Int. Ed.* **2003**, *42*, 5556−5573.

(10) Cuerva, J. M.; Justicia, J.; Oller-López, J. L.; Oltra, J. E. *Top. Curr. Chem.* **2006**, *264*, 63−92.

(11) Gansäuer, A.; Fan, C.-A.; Justicia, J.; Worgull, D. *Top. Curr. Chem.* **2007**, *279*, 25−52.

(12) Gansäuer, A.; Pierobon, M.; Bluhm, H. *Angew. Chem., Int. Ed.* **1998**, *37*, 101−103.

Scheme 2. Schematic Mechanistic Picture for Epoxide Opening

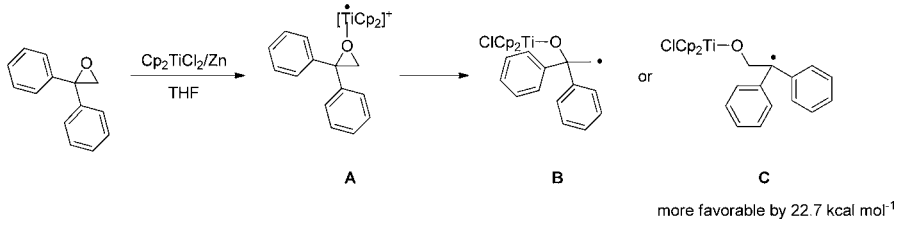

(13) Gansäuer, A.; Bluhm, H.; Pierobon, M. *J. Am. Chem. Soc.* **1998**, *120*, 12849−12859.
(14) Barrero, A. F.; Rosales, A.; Cuerva, J. M.; Oltra, J. E. *Org. Lett.* **2003**, *5*, 1935−1938.
(15) Justicia, J.; Rosales, A.; Buñuel, E.; Oller-López, J. L.; Valdivia, M.; Haïdour, A.; Oltra, J. E.; Barrero, A. F.; Cárdenas, D. J.; Cuerva, J. M. *Chem.—Eur. J.* **2004**, *10*, 1778−1788.
(16) Gansäuer, A.; Lauterbach, T.; Bluhm, H.; Noltemeyer, M. *Angew. Chem., Int. Ed.* **1999**, *38*, 2909−2910.
(17) Gansäuer, A.; Bluhm, H.; Lauterbach, T. *Adv. Synth. Catal.* **2001**, *343*, 785−787.
(18) Gansäuer, A.; Bluhm, H.; Rinker, B.; Narayan, S.; Schick, M.; Lauterbach, T.; Pierobon, M. *Chem.—Eur. J.* **2003**, *9*, 531−542.
(19) Gansäuer, A.; Fan, C.-A.; Keller, F.; Keil, J. *J. Am. Chem. Soc.* **2007**, *129*, 3484−3485.
(20) Gansäuer, A.; Fan, C.-A.; Keller, F.; Karbaum, P. *Chem.—Eur. J.* **2007**, *13*, 8084−8090.
(21) Gansäuer, A.; Fan, C.-A.; Piestert, F. *J. Am. Chem. Soc.* **2008**, *130*, 6916−6917.
(22) Gansäuer, A.; Lei, S.; Otte, M. *J. Am. Chem. Soc.* **2010**, *132*, 11858−11859.
(23) Justicia, J.; Oltra, J. E.; Cuerva, J. M. *J. Org. Chem.* **2004**, *69*, 5803−5806.
(24) Justicia, J.; Oller-Lopez, J. L.; Campaña, A. G.; Oltra, J. E.; Cuerva, J. M.; Buñuel, E.; Cárdenas, D. J. *J. Am. Chem. Soc.* **2005**, *127*, 14911−14921.
(25) Justicia, J.; Oltra, J. E.; Cuerva, J. M. *J. Org. Chem.* **2005**, *70*, 8265−8272.
(26) Justicia, J.; de Cienfuegos, L. Á.; Camapaña; Miguel, D.; Jakoby, V.; Gansäuer, A.; Cuerva, J. M. *Chem. Soc. Rev.* **2011**, *40*, 3525−3537.
(27) Jiménez, T.; Morcillo, S. P.; Martín-Lasanta, A.; Collado-Sanz, D.; Cárdenas, D. J.; Gansäuer, A.; Justicia, J.; Cuerva, J. M. *Chem.—Eur. J.* **2012**, *18*, 12825−12833.
(28) Gansäuer, A.; Lauterbach, T.; Geich-Gimbel, D. *Chem.—Eur. J.* **2004**, *10*, 4983−4990.
(29) Friedrich, J.; Dolg, M.; Gansäuer, A.; Geich-Gimbel, D.; Lauterbach, T. *J. Am. Chem. Soc.* **2005**, *127*, 7071−7077.
(30) Friedrich, J.; Walczak, K.; Dolg, M.; Piestert, F.; Lauterbach, T.; Worgull, D.; Gansäuer, A. *J. Am. Chem. Soc.* **2008**, *130*, 1788−1796.
(31) Gansäuer, A.; Worgull, D.; Knebel, K.; Huth, I.; Schnakenburg, G. *Angew. Chem., Int. Ed.* **2009**, *48*, 8882−8885.
(32) Gansäuer, A.; Knebel, K.; Kube, C.; van Gastel, M.; Cangönül, A.; Daasbjerg, K.; Hangele, T.; Hülsen, M.; Dolg, M.; Friedrich, J. *Chem.—Eur. J.* **2012**, *18*, 2591−2599.
(33) Gansäuer, A.; Rinker, B.; Pierobon, M.; Grimme, S.; Gerenkamp, M.; Mück-Lichtenfeld, C. *Angew. Chem., Int. Ed.* **2003**, *42*, 3687−3690.
(34) Gansäuer, A.; Rinker, B.; Ndene-Schiffer, N.; Pierobon, M.; Grimme, S.; Gerenkamp, M.; Mück-Lichtenfeld, C. *Eur. J. Org. Chem.* **2004**, 2337−2351.
(35) Gansäuer, A.; Fleckhaus, A.; Alejandre Lafont, M.; Okkel, A.; Kotsis, K.; Anoop, A.; Neese, F. *J. Am. Chem. Soc.* **2009**, *131*, 16989−16999.
(36) Gansäuer, A.; Behlendorf, M.; von Laufenberg, D.; Fleckhaus, A.; Kube, C.; Sadasivam, D. V.; Flowers, R. A., II *Angew. Chem., Int. Ed.* **2012**, *51*, 4739−4742.
(37) Gansäuer, A.; Klatte, M.; Brändle, G. M.; Friedrich, J. *Angew. Chem., Int. Ed.* **2012**, *51*, 8891−8894.
(38) Nugent, W. A.; RajanBabu, T. V. *J. Am. Chem. Soc.* **1988**, *110*, 8561−8562.
(39) RajanBabu, T. V.; Nugent, W. A. *J. Am. Chem. Soc.* **1989**, *111*, 4525−4527.
(40) RajanBabu, T. V.; Nugent, W. A.; Beattie, M. S. *J. Am. Chem. Soc.* **1990**, *112*, 6408−6409.
(41) RajanBabu, T. V.; Nugent, W. A. *J. Am. Chem. Soc.* **1994**, *116*, 986−997.
(42) Rosales, A.; Oller-López, J. J.; Gansäuer, A.; Oltra, J. E.; Cuerva, J. M. *Chem. Commun.* **2004**, 2628−2629.
(43) Fleury, L. M.; Ashfeld, B. M. *Org. Lett.* **2009**, *24*, 5670−5673.
(44) Estévez, R. E.; Justicia, J.; Bazdi, B.; Fuentes, N.; Paradas, M.; Choquesillo-Lazarte, D.; Garciá-Ruiz, J. M.; Robles, R.; Gansäuer, A.; Cuerva, J. M.; Oltra, J. E. *Chem.—Eur. J.* **2009**, *15*, 2774−2791.
(45) Muñoz-Bascon, J.; Sancho-Sanz, I.; Álvarez-Manzanedo, E.; Rosales, A.; Oltra, J. E. *Chem.—Eur. J.* **2012**, *18*, 14479−14486.
(46) Gianino, J. B.; Ashfeld, B. L. *J. Am. Chem. Soc.* **2012**, *134*, 18217−18220.
(47) Fleury, L. M.; Kosal, A. D.; Masters, J. T.; Ashfeld, B. L. *J. Org. Chem.* **2013**, *78*, 253−269.
(48) Streuff, J.; Feurer, M.; Bichovski, P.; Frey, G.; Gellrich, U. *Angew. Chem., Int. Ed.* **2012**, *51*, 8661−8664.
(49) Streuff, J. *Synlett* **2013**, 276−280.
(50) Asandei, A. D.; Moran, I. W. *J. Am. Chem. Soc.* **2004**, *126*, 15932−15933.
(51) Asandei, A. D.; Chen, Y.; Saha, G.; Moran, I. W. *Tetrahedron* **2008**, *64*, 11831−11838.
(52) Daasbjerg, K.; Svith, H.; Grimme, S.; Gerenkamp, M.; Mück-Lichtenfeld, C.; Gansäuer, A.; Barchuk, A.; Keller, F. *Angew. Chem., Int. Ed.* **2006**, *45*, 2041−2044.
(53) Gansäuer, A.; Barchuk, A.; Keller, F.; Schmitt, M.; Grimme, S.; Gerenkamp, M.; Mück-Lichtenfeld, C.; Daasbjerg, K.; Svith, H. *J. Am. Chem. Soc.* **2007**, *129*, 1359−1371.
(54) Mims, W. B. *Phys. Rev. B* **1972**, *6*, 3543−3545.
(55) Mims, W. B. *Phys. Rev. B* **1972**, *5*, 2409−2419.
(56) Mims, W. B.; Peisach, J. *Biochemistry* **1976**, *15*, 3863−3869.
(57) Mims, W. B. *Proc. R. Soc. London, Ser. A* **1965**, *283*, 452−457.
(58) Davies, E. R. *Phys. Lett. A* **1974**, *47*, 1−2.
(59) Gemperle, C.; Sorensen, O. W.; Schweiger, A.; Ernst, R. R. *J. Magn. Reson.* **1990**, *87*, 502−515.
(60) Arroyo, C. M.; Kramer, J. H.; Leiboff, R. H.; Mergner, G. W.; Dickens, B. F.; Weglicki, W. B. *Free Radicals Biol. Med.* **1987**, *3*, 313−316.
(61) Tsai, P.; Elas, M.; Parasca, A. D.; Barth, E. D.; Mailer, C.; Halpern, H. J.; Rosen, G. M. *J. Chem. Soc., Perkin Trans. 2* **2001**, 875−880.
(62) Reszka, K. J.; McCormick, M. L.; Buettner, G. R.; Hart, C. M.; Britigan, B. E. *Nitric Oxide* **2006**, *15*, 133−141.
(63) Alvarez, M. N.; Peluffo, G.; Folkes, L.; Wardman, P.; Radi, R. *Free Radical Biol. Med.* **2007**, *43*, 1523−1533.
(64) Alberti, A.; Macciantelli, D. In *Electron Paramagnetic Resonance: A Practitioner's Toolkit*; Brustolon, M., Giamello, E., Eds.; Wiley: Hoboken, NJ, 2009.
(65) Williams, D. B. G.; Lawton, M. *J. Org. Chem.* **2010**, *75*, 8351−8354.
(66) Lambert, J. B.; Finzel, R. B. *J. Am. Chem. Soc.* **1983**, *105*, 1954−1958.
(67) Doyle, G.; Tobias, R. S. *Inorg. Chem.* **1967**, *6*, 1111−1115.
(68) Frohn, M.; Wang, Z. X.; Shi, Y. *J. Org. Chem.* **1998**, *63*, 6425−6426.
(69) Mims, W. B.; Peisach, J. *J. Chem. Phys.* **1978**, *69*, 4921−4930.
(70) Neese, F. *ORCA: An ab Initio, DFT and semiempirical SCF-MO package*, 2.9.0 R3002; MPI for Chemical Energy Conversion: Mülheim an der Ruhr, Germany, 2013.
(71) Eichkorn, K.; Treutler, O.; Ohm, H.; Haser, M.; Ahlrichs, R. *Chem. Phys. Lett.* **1995**, *242*, 652−660.
(72) Eichkorn, K.; Weigend, F.; Treutler, O.; Ahlrichs, R. *Theor. Chem. Acc.* **1997**, *97*, 119−124.
(73) Schäfer, A.; Horn, H.; Ahlrichs, R. *J. Chem. Phys.* **1992**, *97*, 2571−2577.
(74) Neese, F. *J. Chem. Phys.* **2001**, *115*, 11080−11096.
(75) Neese, F. *J. Chem. Phys.* **2003**, *118*, 3939−3948.
(76) Symons, M. C. R.; Mishra, S. P. *J. Chem. Soc., Dalton Trans.* **1981**, 2258−2262.
(77) Samuel, E.; Vedel, J. *Organometallics* **1989**, *8*, 237−241.
(78) Burlakov, V. V.; Dolgushin, F. M.; Yanovsky, A. I.; Struchkov, Yu. T.; Shur, V. B.; Rosenthal, U.; Thewalt, U. *J. Organomet. Chem.* **1996**, *522*, 241−247.

(79) Gansäuer, A.; Behlendorf, M.; Cangönül, A.; Kube, C.; Cuerva, J. M.; Friedrich, J.; van Gastel, M. *Angew. Chem., Int. Ed.* **2012**, *51*, 3266−3270.
(80) Samuni, A.; Krishna, C. M.; Riesz, P.; Finkelstein, E.; Russo, A. *Free Radical Biol. Med.* **1989**, *6*, 141−148.
(81) Migita, C. T.; Migita, K. *Chem. Lett.* **2003**, *32*, 466−467.
(82) Zhao, H. T.; Joseph, J.; Zhang, H.; Karoui, H.; Kalyanaraman, B. *Free Radical Biol. Med.* **2001**, *31*, 599−606.
(83) Gansäuer, A.; Franke, D.; Lauterbach, T.; Nieger, M. *J. Am. Chem. Soc.* **2005**, *127*, 11622−11623.